Princeton/HEP/94-19

Proposal for a Wire Chamber-Based CsI Photocathode for a B-Factory RICH

Eric Prebys

Joseph Henry Laboratories, Princeton University

January 19, 1994

Abstract

A design is considered for a CsI photocathode incorporating a proportional wire anode plane. This would have the advantage over the previously considered mesh anode or near wire anode that the anode wires could be moved further away from the cathode pads, allowing position to be determined using interpolation of imaged charge. This would enable comparable or superior position resolution with larger pads, ultimately reducing the channel count. Another advantage would be that the larger gap would simplify the mechanical design and reduce the risk of electrical breakdown, particularly when compared to the mesh-anode design, which behaves as a parallel plate chamber. This note discusses the optimum design parameters (spacing, gas-gain, etc) and estimated performance for such a scheme.

1 Introduction

Many of the fast-RICH designs considered for B-Factory detectors utilize a photocathode consisting of cesium iodide (CsI) evaporated onto a copper cathode plane. The Cherenkov photons striking the cathode plane release photoelectrons, which are amplified via an avalanche process. The resulting charge is imaged onto the cathode plane, which is segmented into pads which are read out.

In the majority of the current designs, the avalanche field is generated either by a mesh anode plane or an anode plane consisting of wires positioned very close (1-2 mm) to the cathode plane. This is because these designs were originally conceived for hadronic machines where speed was an issue, as was "blindness" to the passage of ionizing particles. These issues are less important at the B-factory.

One problem with these designs is that because of the small gap between the anode and the cathode, the lateral profile of the image charge is very narrow, so the spatial resolution is generally limited by the pad size

$$\sigma_p = \frac{w}{\sqrt{12}} \tag{1}$$

where p is the position in one dimension and w is the width of a pad. Good spatial resolution requires small pads and therefore large channel counts.

The solution considered here is to collect the photoelectrons in a wire chamber-like configuration, as shown in figure 1. In this configuration, the gap between the anode and the cathode can be increased so that the image charge spreads over several pads, allowing position interpolation with resolution down to a small fraction of the pad size. Therefore larger pads could be used and still enable comparable spatial resolution.

Another issue is electrical breakdown, particularly in the case of the mesh-anode designs. The detector described in [1] was initially based on a parallel plate type Cherenkov detector and experienced breakdown even at very low gains due to the presence of low-energy, highly ionizing particles. The problem was so bad that it was ultimately converted to a MWPC-based design, which solved the problem. Granted, this detector was for a heavy ion, fixed target experiment where this sort of background was more of an issue issue. Still, it is somewhat disturbing. This will be discussed in more detail in section 8.

2 Design Goals

Figure 2 shows the most likely configuration for the KEK B-Factory RICH. A 10mm C_6F_{14} (n=1.273) radiator is followed by a 200 mm expansion region[1], after which the Cherenkov photons are detected by the photocathode. For a particle with $\beta \approx 1$, the Cherenkov angle in the radiator is $\theta_C = \cos^{-1}(1/n) \approx 38°$, giving an angle in the expansion volume of $\theta'_C = \sin^{-1}(n \sin(\theta_C)) \approx 52°$. For normal incidence, light exits the radiator in a circle of radius $\delta = t \tan(\theta_C) \approx 8$ mm. The width of this ring is one

[1]In fact, the current baseline design allows for only a 150 mm expansion region, but we feel the amount of space required for the electronics can be reduced, particularly if we can reduce the channel count. This would allow for a longer expansion region.

limit on the angular resolution. Another limit is the chromaticity, ie the fact that the index of refraction of the radiator varies with frequency. The latter gives a position uncertainty at the radiator (see Appendix A) of $\sigma_r \approx 4$ mm. The irreducible position uncertainty (σ_p) at the photocathode is therefore given by

$$\sigma_p^2 = \sigma_r^2 + \frac{\delta^2}{12} \tag{2}$$

or in this case σ_p ≈4.5 mm. This is large compared to the intrinsic resolution of of the current pads, $\sigma_p = w/\sqrt{12}$, where w is the pad pitch - 8 mm in the current baseline, giving a position resolution of 2.2 mm. Therefore the goal is to achieve similar position resolution - say 2 mm, while increasing the pad pitch by on the order of a factor of two, thereby reducing the channel count by four.

3 Image Charge Distribution

In one direction, the spatial resolution will ultimately be limited by the anode wire spacing, so the anode wires will necessarily be close together. Therefore it is appropriate to use the charge distribution calculated in the $s/d << 1$ limit, where s is the wire spacing and d is the gap between the anode and the cathode. In the this limit, the image charge distribution on the cathode in one direction is given by[2]

$$\Gamma(\lambda) = \frac{\pi}{8}\mathrm{sech}^2\left(\frac{\pi\lambda}{2}\right) \tag{3}$$

where $\lambda = x/d$, x being the direction along the cathode. Figure 3 shows this distribution. The total charge collected on one cathode is of course half of the total charge.

4 Position Determination

To simplify pattern recognition, it is desirable that most of the charge be contained in a 3×3 cell about the point of incidence of the photon. The position can then be found by forming 3 pad "pseudostrips" in each dimension and interpolating the position. The most straightforward way to do this is to find the center of gravity in each dimension and then correct this for non-linearities. Figure 4 shows the true electron position (x_t) vs the mean as determined from three strips (x_m) for various values of d/w. Positions are given in units of strip width. When d/w is small, most of the charge is deposited in a single pad. When d/w is large, not all the charge is

contained in three strips. At each point, the error in the position is given by

$$\Delta_{x_t} = \left(\frac{dx_t}{dx_m}\right) \Delta_{x_m} \tag{4}$$

The error on the mean at each position is given by

$$\sigma^2_{x_m} = \left(\frac{\sigma'_Q}{Q}\right)^2 \sum_{i=1}^{3} (x_i - x_m)^2 \tag{5}$$

where Q is the total charge collected and σ'_Q is the noise in one pseudostrip ($= \sqrt{3}\sigma_Q$, where σ_Q is the noise in one pad). The average error is then given by

$$\begin{aligned} \sigma^2_x &= \left(\frac{\sigma'_Q}{Q}\right)^2 \int_{-1/2}^{1/2} \sum_{i=-1}^{1} (i - x_m)^2 \left(\frac{dx_t}{dx_m}\right)^2 dx_t \\ &\equiv \left(\frac{\sigma'_Q}{Q}\right)^2 \mathrm{C}(d')^2 \end{aligned} \tag{6}$$

where $d' = d/w$. Values for C are calculated numerically and plotted in figure 5 as a function of d'. It is seen that there is a minimum at about d'=.7, with reasonable values in the range $.5 < d' < 1$. The function rises steeply below d'=.5 because most of the charge is often in one strip. At $d' = .7$, C≈ 1.6.

5 Avalanche Profile

The distribution of avalanches produced by single electrons in high fields follows the so-called Polya distribution[3]

$$\mathrm{P}(a) \propto a^{b-1} \mathrm{e}^{-ba} \tag{7}$$

where $a \equiv G/\bar{G}$, G being the gain for a particular electron and $\bar{G}$ being the mean gain of the system. b is related to the width of the distribution ($(\sigma_a/a)^2 = 1/b$). Using $b = 3/2$ gives a reasonably good description of a wide range of gases. Figure 6a is normalized Polya distribution with $b = 3/2$. Note that there is an abundance of signals below the mean value. Figure 6b shows the efficiency as a function of the cut on signal height and it it seen that in order to get a 95% efficiency, one must place the cut at about 10% of the mean signal.

This wide, non-gaussian distribution implies that when one is calculating the average uncertainty in the weighted mean, one cannot use the mean gain ($\bar{G}$), but rather a modified gain ($\tilde{G}$), given by

$$\frac{1}{\tilde{G}^2} = \frac{1}{\bar{G}^2}\frac{\int_{a_c}^{\infty}\frac{1}{a^2}\mathrm{P}(a)da}{\int_{a_c}^{\infty}\mathrm{P}(a)da} \equiv \frac{1}{\bar{G}^2}\mathrm{K}(a_c) \quad (8)$$

where a_c is the threshold signal over the mean signal. For $b = 3/2$ the integral $\mathrm{K}(a_c)$ is

$$\mathrm{K}(a_c) = \frac{6\mathrm{e}^{-\frac{3}{2}a_c}}{\epsilon(a_c)}\sqrt{\frac{3}{2\pi}}\left(\frac{1}{\sqrt{a_c}} + 3\sqrt{a_c}\right) - 9 \quad (9)$$

where $\epsilon(a_c)$ is the efficiency of signal detection at a cut of a_c. For $a_c = .1$ ($\epsilon(.1) \approx .95$), K$\approx$ 6.5. This implies that the appropriate gain to use when estimating the average position uncertainty is

$$\tilde{G} = \frac{\bar{G}}{\sqrt{\mathrm{K}(a_c)}} \approx \frac{\bar{G}}{2.5} \quad (10)$$

6 Determination of Parameters

Plugging in everything that has been derived up to now, the expression for the position resolution becomes

$$\sigma_x = \mathrm{C}(d')\frac{\sigma'_Q}{\frac{1}{2}\tilde{G}} \quad (11)$$

where the factor of 1/2 in front of $\tilde{G}$ is due to the fact that only half the charge is seen on the imaging cathode. Expanding this out, one gets

$$\sigma_x = \mathrm{C}(d')\frac{2\sqrt{\mathrm{K}(a_c)}\sqrt{3}\sigma_Q}{\bar{G}} \quad (12)$$

Assuming an optimum C$\approx$ 1.6 and a realistic electronic noise per channel of $\sigma_Q \approx$ 2000e, gives the relationship

$$\frac{\sigma_p}{w} \approx \frac{2.8 \times 10^4}{\bar{G}} \quad (13)$$

where here the normalized unit x has been converted back to the absolute unit p by multiplying by the strip width.

Taking our desired goal of a position resolution of 2 mm and a pad size of 16 mm,(13) gives a mean gas gain of 2.5×10^5. However, other considerations warrant a slightly higher gas gain. If one uses a 3×3 sum to find hits on the photocathode,

then the effective noise will be $3\sigma_Q \approx 6000e$. The electronic threshold will be set at $\approx \frac{1}{2} a_c \bar{G}$, so to get a 4σ discriminating power again requires a gain of $\bar{G} \approx 5 \times 10^5$. At this gas gain, one could go to even larger pads, however because this gain is a bit of a stretch, it is probably better to err on the side of conservatism.

A pad size of 16 mm implies an optimum anode distance to the anode of $.7 \times 16 =$ 11 mm, however similar performance should be achieved with a gap down to 8 mm.

7 Anode Wire Spacing

Since the avalanche will always occur at a wire, the resolution in one direction is limited by the anode wire spacing. If the wire spacing is small compared to the pad size, then the corrected spatial resolution is given by

$$\sigma_p'^2 = \sigma_p^2 + \frac{s^2}{12} \tag{14}$$

where s is the anode wire pitch. Assuming that $\sigma_p \approx 2$ mm, then if one wants at most 10% degradation in σ_p', one can go up to wire spacings of 3.2 mm.

8 Gas and Breakdown Issues

It is very important that the chamber gas be UV transparent. The required gain (5×10^5) is also rather high for a gas at atmospheric pressure. Gases considered to date usually consist of helium with a small admixture of an organic quenching agent. For example, mixtures of 95%H and 5% CH_4 or C_2H_6, have been shown to give stable operation up to gains of 5×10^5 in parallel plate geometries[4].

In a previously cited work[1], a problem was mentioned with breakdowns using parallel-plate chamber geometries in a real experiment. Those authors found that the breakdown condition depended on the *total charge* present during an avalanche, rather than on the absolute gain. It was found that breakdown occurred for values of $n_0 M > 10^8$ where n_0 is the initial number of electron-ion pairs, and M is the average gas gain. Thus, very highly ionizing particles caused breakdowns even at relatively low gains. In particular, slow protons can deposit up to 8000 electrons for a similar gap in a similar gas. This limits the gain to a little over 10^4.

In contrast, in MPWC's the relevant number was found to be as high as $2-3\times10^9$, perhaps even higher when TMAE is not used. This points to a safe maximum gain of at least several 10^5.

Of course, slow protons shouldn't be a problem in a B-Factory detector. Still, for such an important part of the apparatus, it is important to keep the design as conservative as possible.

9 Dynamic Range

It's reasonable to set least significant bit (LSB) to something like half the electronic noise, so that quantization error is negligible. The higher end of the range is determined by the largest signal that is likely to be seen. Based on figure 6a, it appears that the range should extend to cover about 5 times the average gain. The maximum signal seen in a single pad with $d' = .5$ is about 85% of the total, so the required dynamic range is

$$R = \frac{\frac{1}{2} \times .85 \times 5 \times \bar{G}}{\frac{1}{2} \times \sigma_Q} \tag{15}$$

where the factor of 1/2 in front of the gain is due to the fact that only half the charge is seen on the cathode. Using $\sigma_Q = 2000$ and $\bar{G} = 5 \times 10^5$ gives

$$R = 1063 \tag{16}$$

or about 10 bits minimum. Note that even if the central strip saturates, at such large signals the two side strips should still give quite good position resolution.

10 Summary and Conclusions

After initial investigation, it seems possible that by using photocathode based on a multi-wire proportional chamber along with analog readout of the cathode pads, one can improve the position resolution relative to one based on a near anode even with pads which are a factor of two larger. The optimum parameters for such a chamber are summarized below

- w - pad pitch $\approx$ 16 mm
- d - anode/cathode gap $\approx$ 8-10 mm
- s - anode wire spacing $\approx$ 3 mm
- G - average gas gain $\approx 5 \times 10^5$
- dynamic range $\approx$ 10 bits

This provides a position resolution of < 2 mm, while reducing the total channel count by a factor of four.

One worry about such a scheme is the high gas gain (5×10^5). This gain is at the limit of what has been achieve reliably in this sort of configuration. The desired resolution can be maintained down to gas gains of about half this value, but electronic

noise begins to become an issue in pattern recognition. Work is going on to determine if it is feasible to operate this chamber at such high gains.

This design also has the complication that it requires an analog readout rather than the pixel readout of some of the other designs; however, it can be argued that analog readout is a conservative approach that should be implemented anyway.

A Chromaticity

One of the major contributions to the Cherenkov angular resolution is chromaticity - the fact that the index of refraction depends on the photon frequency. In the region of interest, the frequency dependence of the index of the C_6F_{14} radiator has been measured to be [5]

$$\mathrm{n}(\nu) = 1.2733 + .0093 \times (h\nu - 6\mathrm{eV}) \tag{17}$$

where ν is the photon frequency and h is the Planck constant. The effect is small enough that the initial production of photons is still flat in frequency. However, the frequency dependence of the index of refraction causes angular deviations, both in the production of the Cherenkov light, and in the refraction at the boundary to the expansion region. For normal incidence, the radius of light at the photocathode is (referring to figure 2)

$$\begin{aligned} r &= l \tan(\theta_c') \\ &= l \tan\left(\sin^{-1}\left(\mathrm{n}(\nu)\sin\left(\theta_c\right)\right)\right) \\ &= l \tan\left(\sin^{-1}\left(\mathrm{n}(\nu)\sin\left(\cos^{-1}\left(\frac{1}{\mathrm{n}(\nu)\beta}\right)\right)\right)\right) \end{aligned} \tag{18}$$

where the thickness of the radiator has been ignored for the moment. For very relativistic particles, this becomes just a function of ν ($r \approx \mathrm{r}(\nu)$). The average radius is then given by

$$\bar{r} = \frac{\int_{\nu_0}^{\nu_1} \mathrm{r}(\nu)\epsilon(\nu)d\nu}{\int_{\nu_0}^{\nu_1} \epsilon(\nu)d\nu} \tag{19}$$

where $[\nu_0, \nu_1]$ is the frequency range of interest and $\epsilon(\nu)$ is the overall transport and detection efficiency for the photons. The variance of the radius is

$$\sigma_r^2 = \frac{\int_{\nu_0}^{\nu_1} \left(\mathrm{r}(\nu) - \bar{r}\right)^2 \epsilon(\nu)d\nu}{\int_{\nu_0}^{\nu_1} \epsilon(\nu)d\nu} \tag{20}$$

The cutoff for photons in the C_6F_{14} radiator is about $h\nu = 7.2$ eV[5]. The efficiency of the Cesium iodide photocathode can be approximated as zero below $h\nu = 6$ eV

followed by a linear rise up to the cutoff[6]. Numerically solving (19) and (20) using $l = 200$ mm and the approximate efficiency just described gives

$$\bar{r} = 266.6 \text{ mm} \tag{21}$$

and

$$\sigma_r = 3.9 \text{ mm} \tag{22}$$

References

[1] B.Baur, *et al*, *In-Beam Experience from the CERES UV-Detectors: Prohibitive Spark Breakdown in Multi-Step Parallel-Plate Chambers as Compared to Wire Chambers*, CERN-PPE/93-169 (1993).

[2] E. Mathieson and J.S. Gordon, *Cathode Charge Distributions in Multiwire Chambers (II)*, Nucl. Inst. and Meth. in Phys. Res. **227** (1984) 277-282.

[3] J. Byrne, *Statistics of the Electron Multiplication Process in Proportional Counters*, Proc. Roy. Soc. Edin. **66A** (1962) 33.

[4] C.Lu, K.T. McDonald, and Y.Zhu, *Helium Gas Mixtures for RICH Detectors with CsI Photocathodes*, Nucl. Inst. and Meth. in Phys. Res. **A334** (1993) 328-338.

[5] R.Arnold, *et al*, *A Ring Imaging Cherenkov Detector, The DELPHI Barrel RICH Prototype (Part B)*, Nucl. Inst. and Meth. in Phys. Res. **A270** (1988) 289-318.

[6] A. Braem, *et al*, *Fast-RICH Detector with a Cesium Iodide Photocathode at Atmospheric Pressure*, CERN-PPE/93-209 (1993) *(Interpretation of figure 12).*

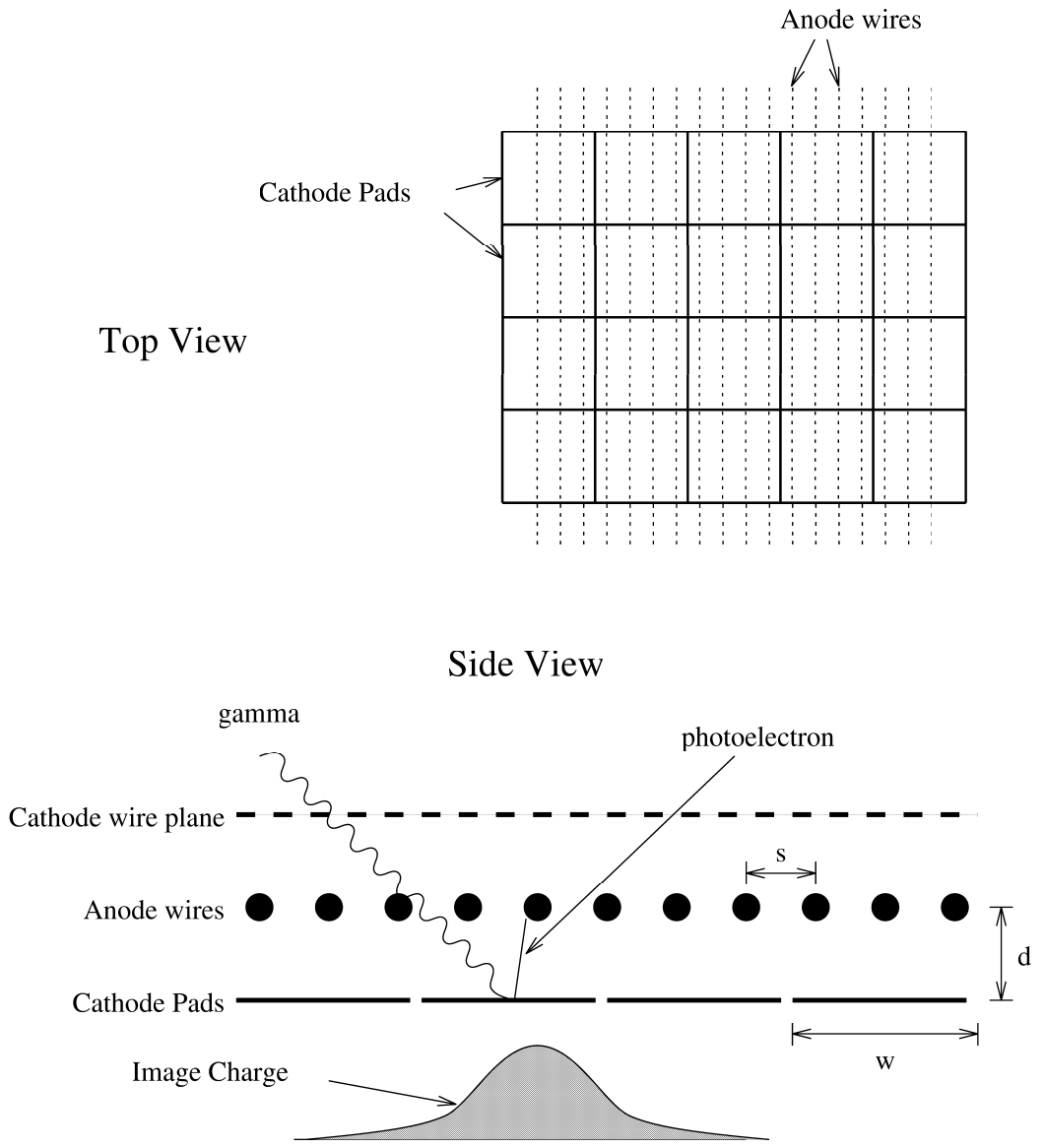

Figure 1: Design of a MWPC-based photocathode. A thin layer of cesium iodide (CsI) is evaporated onto the segmented cathode. X-ray photons create photoelectrons in the CsI, which drift to the anode wires and create avalanches. These avalanches in turn generate image charge on the cathode plane.

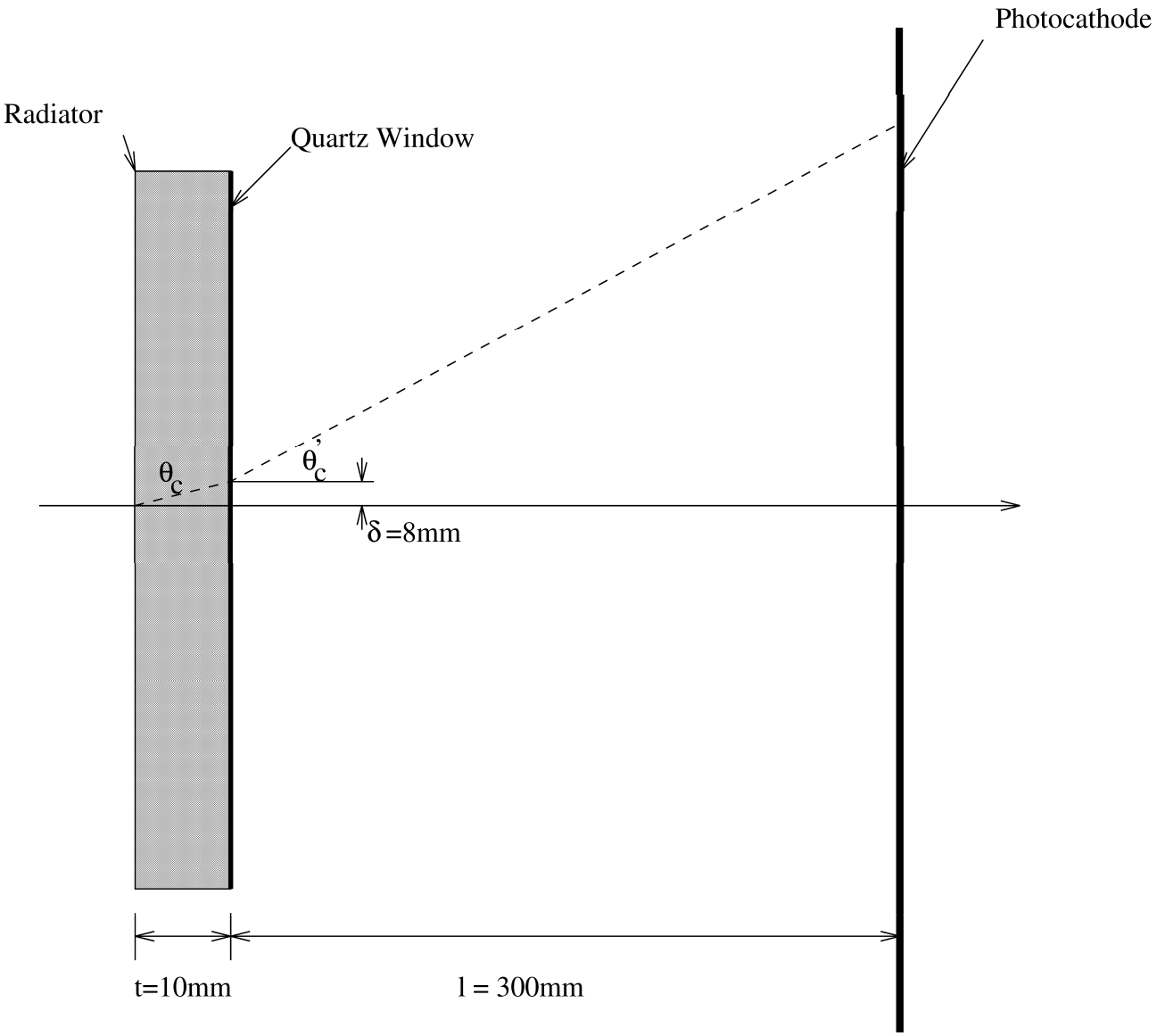

Figure 2: Conceptual layout of the KEK RICH (not to scale). Cherenkov photons are generated in the radiator volume. The expansion region provides lever arm to improve angular resolution of the photons, which are detected at the photocathode plane.

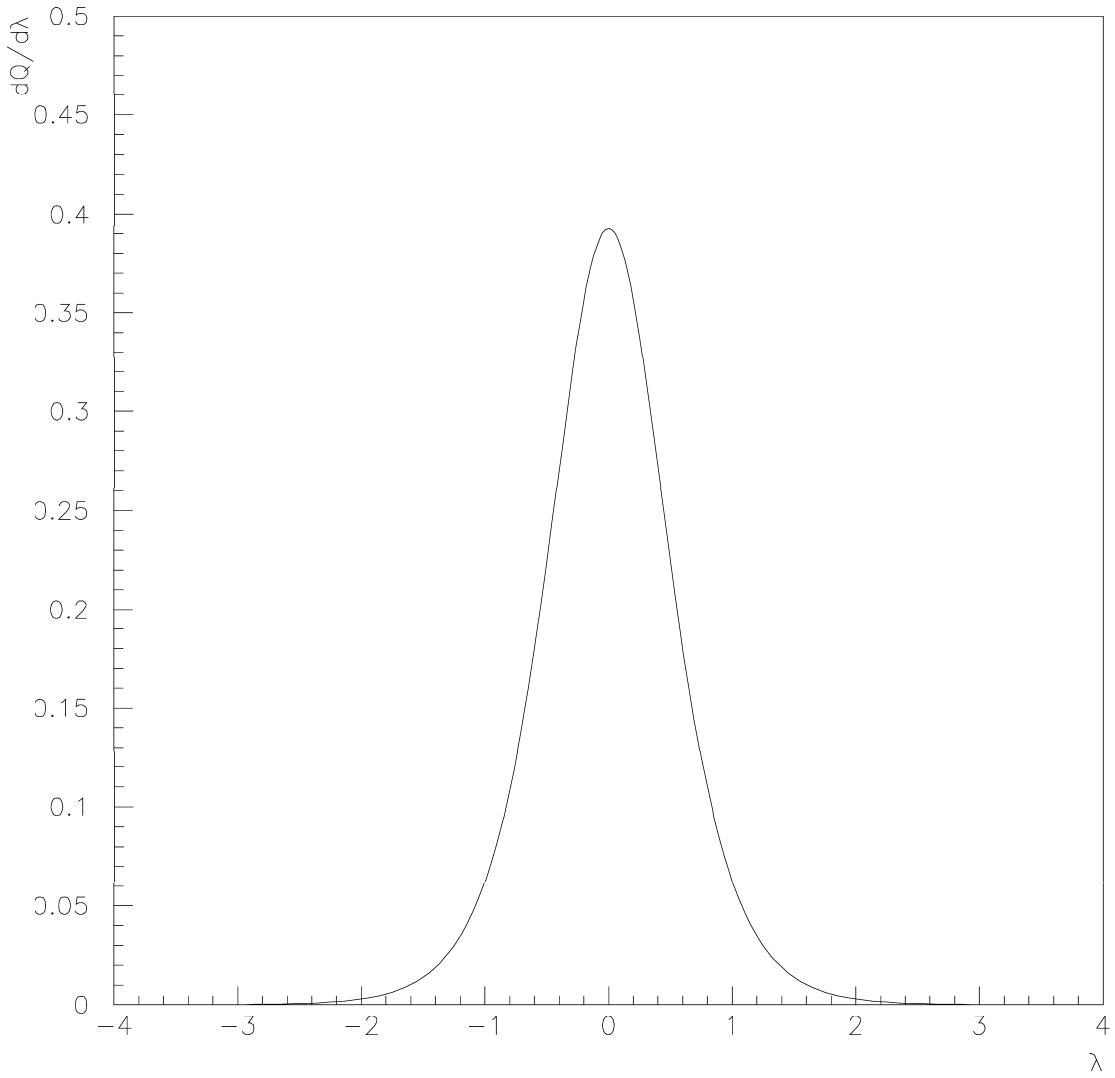

Figure 3: Induced charge distribution on cathode as a function of $\lambda(\equiv x/d)$.

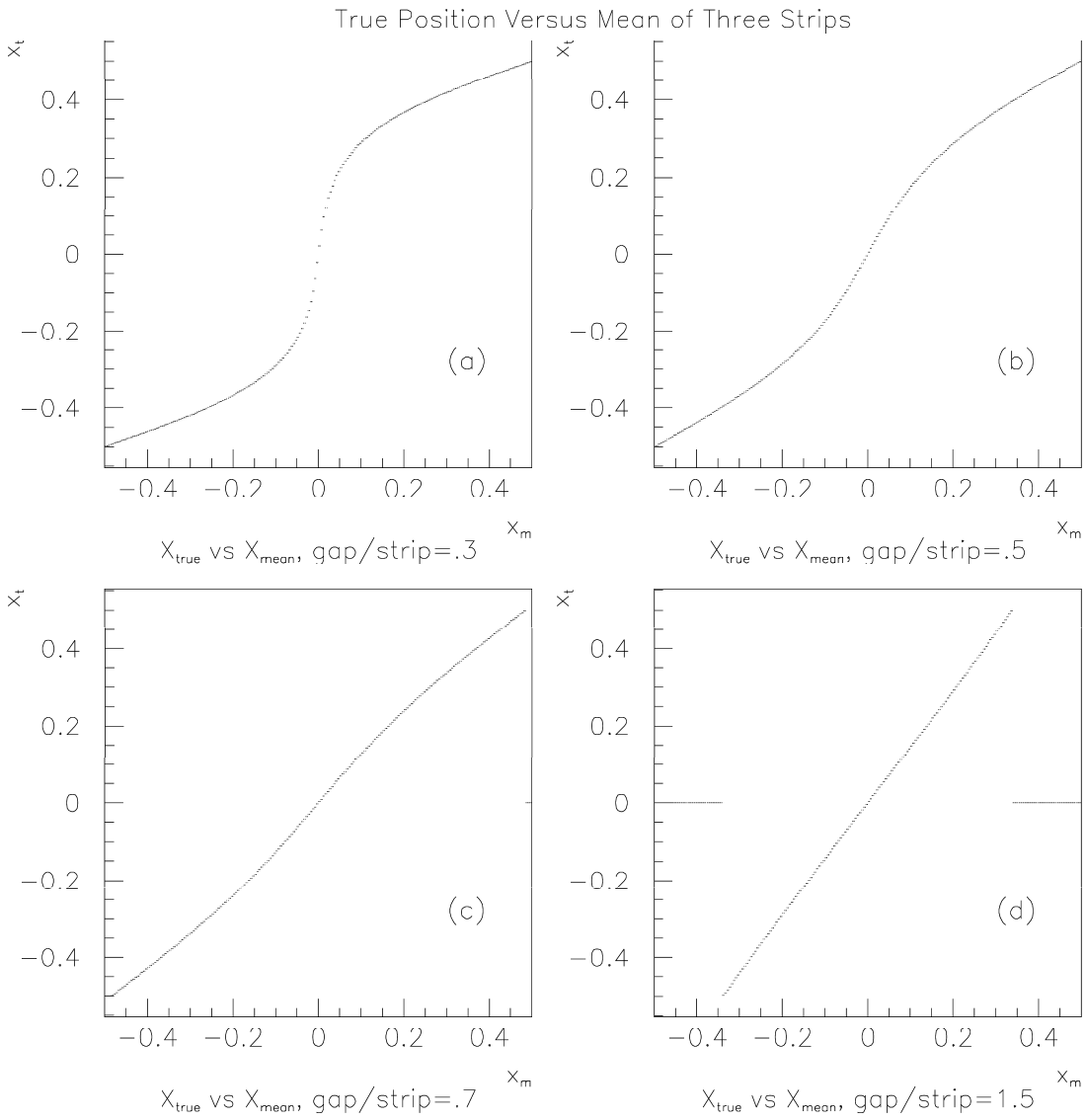

Figure 4: Plot of the true position versus the weighted mean for d/w = (a) .3, (b) .5, (c) .7, and (d) 1.5.

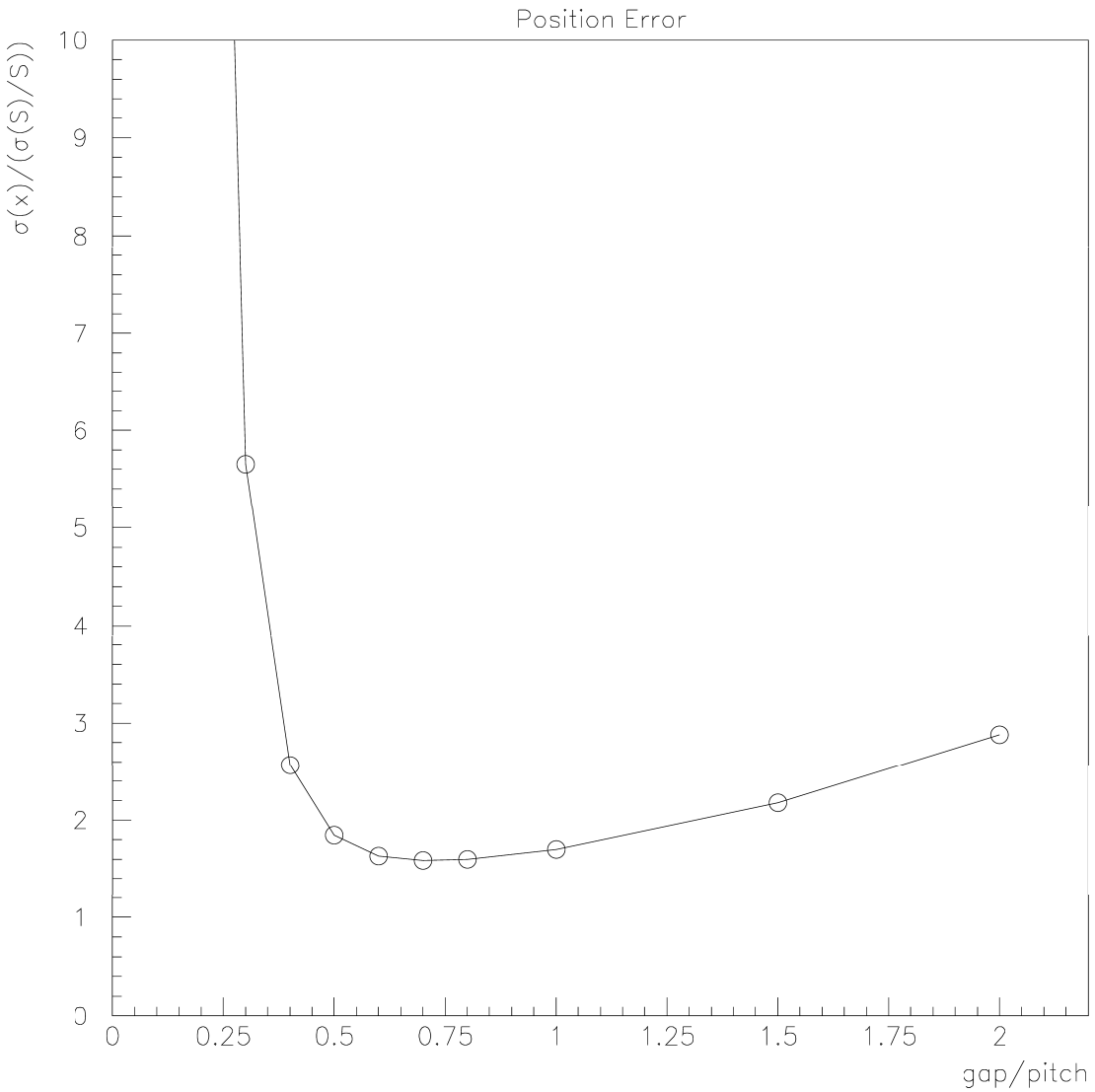

Figure 5: The mean error in position error relative to charge measurement error as a function of d/w.

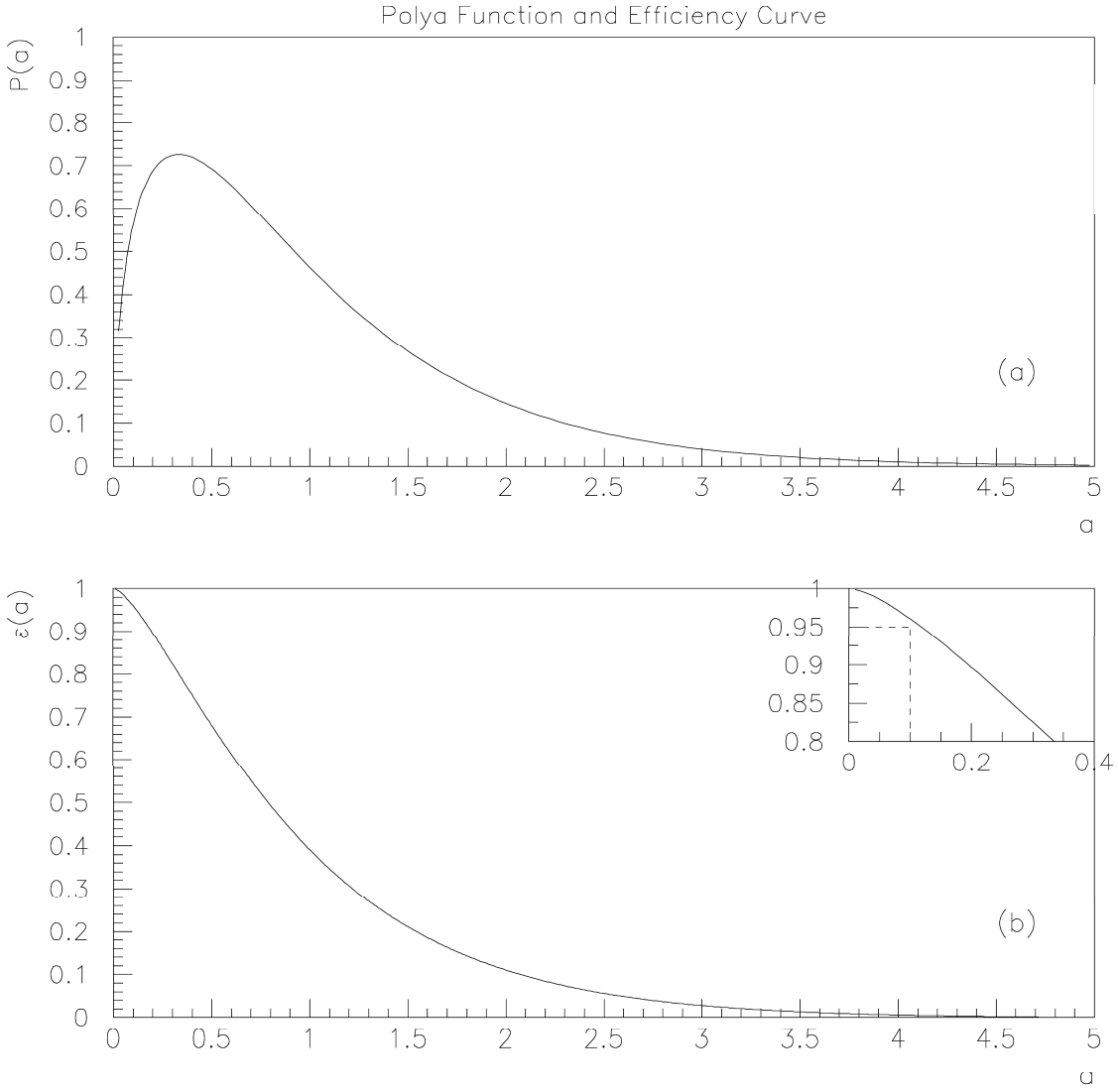

Figure 6: (a) shows the distribution of gains for single electron avalanches normalized to $\bar{G} = 1$. This is the Polya distribution with b=3/2. (b) shows the efficiency as a function of the cut on avalanche height.